Journal of the European Ceramic Society 23 (2003) 721–728

www.elsevier.com/locate/jeurceramsoc

Electrical properties of Sb and Cr-doped $PbZrO_3$–$PbTiO_3$–$PbMg_{1/3}Nb_{2/3}O_3$ ceramics

R.W. Whatmore*, O. Molter, C.P. Shaw

School of Industrial and Manufacturing Sciences, Cranfield University, Cranfield MK43 0AL, UK

Received 12 January 2002; accepted 12 May 2002

Abstract

The pyroelectric, dielectric and DC resistive properties of Sb and Cr-doped ceramics with a base composition of $Pb(Mg_{1/3}Nb_{2/3})_{0.025}(Zr_{0.825}Ti_{0.175})_{0.975}O_3$ have been studied. Sb doping has been shown to produce a linear reduction in Curie temperature ($T_C = -22z + 294$ °C) with concentration (z) and to give an increase in pyroelectric coefficient from 250 to 310 $\mu Cm^{-2}\ K^{-1}$ for z increasing from 0 to 3 at.%. It also produces first a reduction and then an increase in both dielectric constant and loss, so that the 33 Hz pyroelectric figures of merit (FOM's) are as follows: F_V peaks at $3.8\times10^{-2}\ m^2\ C^{-1}$ and F_D peaks at $1.2\times10^{-5}\ Pa^{-1/2}$. The resistivity is increased substantially from 1.1×10^{11} to ca 6×10^{11} Ωm with 1 at.% Sb, thereafter changing little. The behaviour has been explained in terms of Sb acting as a donor ion, reducing oxygen vacancy concentrations up to 1 at.%, with conductivity dominated by hole hopping between traps ($E_a = 0.59 \pm 0.05$ eV) that are not changed by the Sb doping. It is concluded that additions of higher levels of Sb do not produce electron-mediated hopping conduction. The Cr additions have no effect upon T_C, but reduce dielectric constant and loss, pyroelectric coefficient and resistivity at doping levels up to 3 at.%. The FOM F_V peaks at $3.6\times10^{-2}\ m^2\ C^{-1}$ and F_D at $1.9\times10^{-5}\ Pa^{-1/2}$. The behaviour of the electrical resistivity as a function of dopant level is shown to produce a linear $\ln(\sigma_o)$ vs $z^{-1/3}$ dependence (σ_o = DC conductivity), as would be expected for hole hopping conduction between Cr^{3+} sites, with an $E_a = 0.38 \pm 0.03$ eV.

Keywords: Electrical properties; $Pb(Mg,Nb,Zr,Ti)O_3$; Perovskites; PZT

1. Introduction

The use of the pyroelectric effect for the detection of infra-red radiation in the 3–5 and 8–12 μm IR bands has been known for many years[1] and has been extensively commercialised in applications such as people sensing, environmental monitoring and gas analysis.[2] There has also been, for about 25 years, an interest in the development of pyroelectric devices for thermal imaging.[3] Solid state arrays are of particular interest.[4] These use a thin ferroelectric ceramic wafer bonded to a 2D array of amplifiers and multiplexer switches integrated on an application specific silicon integrated circuit (ASIC). Companies such as BAE SYSTEMS Infra-red Ltd. in the UK have developed arrays with 128×256 and 384×288 elements,[3] while Raytheon in the USA have developed an array with 320×240 elements.[5] These arrays with large numbers (ca 100 K) of very small (ca 40 μm) elements provide excellent thermal imaging performance. Typically they use ceramics such as lead scandium tantalate (PST[6]) or barium strontium titanate (BST[7]) operated close to their Curie temperatures and under an electrical bias (so-called ''dielectric bolometer mode''). The combination of high permittivity (ca 2000) and very high pyroelectric coefficient (ca 3500 $\mu Cm^2\ K^{-1}$) with low dielectric loss (ca 5×10^{-3}) under these conditions makes such materials well matched to the very small elements used in thermal imaging.

There is also a need for arrays with a lower resolution capability to address areas such as: spatially-resolved people sensing (e.g. for monitoring people movements, environmental control etc); spatially-resolved flame and fire sensing; security, automotive sensing, traffic monitoring and low resolution imaging radiometry. A recognisable image is not required for these applications, and a relatively small number (e.g. 16×16) of larger (few hundred μm dimension) elements is adequate. There have been attempts to address these applications with arrays

* Corresponding author. Tel.: +44-1234-750759 x4057; fax: +44-1234-751346.

E-mail address: r.w.whatmore@cranfield.ac.uk (R.W. Whatmore).

0955-2219/02/$ - see front matter © 2002 Elsevier Science Ltd. All rights reserved.
PII: S0955-2219(02)00162-0

based upon ferroelectric polymers such as PVDF/TrFE,[8,9] with linear arrays using ferroelectric thin films on MgO[10] and with 2D arrays using ferroelectric thin films directly integrated onto silicon.[11] The performance of the first is inadequate because of the low pyroelectric figures of merit (FOM)[2] of the ferroelectric polymers, the linear arrays require a relatively expensive and bulky optical scanning system to provide the 2D spatial information. The technology for making 2D arrays based upon ferroelectric thin films on silicon is difficult and not yet ready for the market.

Ferroelectric ceramics based on the $PbZr_xTi_{1-x}O_3$ (PZT) system with $x \approx 1$ or 0, offer a combination of pyroelectric figures-of merit that make them ideal for such low resolution arrays,[2,3] possessing moderate permittivities (ca 200–300), low dielectric losses and good pyroelectric properties (ca 300 $\mu Cm^2\ K^{-1}$). A particularly important aspect of the performance of such materials is the control of DC resistivity. (This is in contrast with the fine-pitch arrays using bolometer-mode ceramics, for which high resistivity is essential.) It permits the electrical time constant of the element to be fixed without recourse to an external resistor and it allows the bias point of the input amplifier on the ASIC to be determined. Previous work has shown[12] that uranium is a very effective dopant both to reduce permittivity and loss, and for the control of electrical resistivity in pyroelectric ceramics. This was originally demonstrated for the $PbZrO_3$–$PbTiO_3$–$PbFe_{1/2}Nb_{1/2}O_3$ (PZFNT) system.[13] Compositions close to $PbZrO_3$ in the $PbZrO_3$–$PbTiO_3$–$PbMg_{1/3}Nb_{2/3}O_3$ (PMNZT) system have been shown to possess excellent pyroelectric properties[14,15] and uranium has also been demonstrated to be an effective dopant for the control of electrical resistivity in this system.[16] However, there are potential problems with the acceptability of uranium as a dopant and there is therefore a need to find an effective alternative for resistivity control. The role of uranium as a dopant has been previously reported as being due to its multi-valent donor character,[13] as it possesses a valency of between 4+ and 6+ and substitutes on the perovskite "B" site for ions with an average valency of 4+. The observed behaviour of the electrical resistivity with dopant level (which first increases and then decreases above a doping level of ca 0.2 mol%) has been interpreted as initial compensation for intrinsic acceptor sites caused by loss of PbO, followed by the donated electrons acting as charge carriers, which hop between localised trap-sites. Based on this observation, there is a good case for the examination of other donor dopants for this role. Previous work by Takahashi[17] has shown that donor dopants such as Nb (B-site) and Sb (A-site) generally act to increase the resistivity of morphotropic phase boundary lead zirconate titanate (PZT) compositions, with no evidence for a significant decrease in resistivity at high doping levels. On the other hand, the same paper reports that Cr behaves in a rather similar way to uranium, first increasing and then decreasing the resistivity as the dopant level is increased. This has also been confirmed by other workers.[18] There is thus a good case for a more detailed assessment of single and multi-valent dopants on the electrical properties of pyroelectric ceramics. The study reported here is an assessment of the effects of Sb and Cr in the PMNZT system. The base composition chosen for the study was formulated as $Pb(Mg_{1/3}Nb_{2/3})_{0.025}(Zr_{0.825}Ti_{0.175})_{0.975}O_3$. This was chosen on the basis of earlier studies[14] as having particularly interesting pyroelectric properties.

2. Experimental

Ceramic pellets with the composition $Pb\{(Mg_{1/3}Nb_{2/3})_{0.025}(Zr_{0.825}Ti_{0.175})_{0.975}\}_{1-z}X_zO_3$ (where X = Sb or Cr) were fabricated from 99.9% pure raw materials using a standard mixed-oxide process as described previously.[19] Excess PbO (1 at.%) was added to the formulation to help compensate for PbO losses during processing. Sample densities were all between 94 and 96% theoretical. The samples were polished, immersed for approximately 2 s in a grain boundary etch [HCL 4.5 vol.%/HF 0.5 vol.%/distilled water] and studied using optical microscopy and a Cambridge Instruments scanning electron microscope (SEM) with backscatter detector. The mean grain size was determined using the linear intercept technique proposed by Wurst and Nelson.[20] Evaporated Cr/Au electrodes were applied for the electrical measurements. Resistivity measurements were made on unpoled samples (to avoid confusion between resistive and pyroelectric currents) and under vacuum (to remove surface moisture). A thermoelectric heater/cooler was employed to maintain a constant temperature during the measurement. A constant applied voltage of 2 V was used, with a Keithley 6217 electrometer to measure the resistive current. The temperature was raised from 15 to 65 °C in steps of 10 °C. The current was monitored for 10 min at each temperature and was observed to follow an exponential decay: $i(t) = i_0\ e^{1/t}$ where $i(t)$ is the current at time t and i_0 is the current at infinite time. The values of i_0 were obtained by extrapolation of $\ln(i(t))$ vs $1/t$ and used to compute the DC resistivities discussed below. Unpoled dielectric properties (1 kHz) were measured from 20 up to 300 °C using an HP4192A impedance analyser to obtain the Curie temperatures from the maximum in the permittivity.

Samples were poled under an electric field of 3 kV/mm in hot mineral oil at 120 °C for 10 min, the field being maintained until the oil temperature had cooled to 40 °C. Prior to any measurements, they were placed in an oven at 50 °C overnight with their electrodes shorted to remove any space charges that may have been introduced by the poling process. The dielectric

properties of the poled samples were measured at 1 kHz and 33 Hz using a GenRad 1689 RLC Digibridge. It should be noted that measurement at a low frequency (a few 10s Hz) is very important for any material being considered for use in pyroelectric applications, as this is the frequency range in which most pyroelectric devices are operated. The pyroelectric coefficients were measured under vacuum using the same rig as that used for the DC resistivities. Two techniques were used. The first was the linear temperature ramp (Byer and Roundy[21]) method, whereby the temperature (T) of the sample was raised (or lowered) from 20 to 90 °C at constant rate and the pyroelectric current i_p measured. The pyroelectric coefficient $p(T)$ was computed from $p(T)=i_p/(A.dT/dt)$ (where A is the area of the sample). The second technique was method whereby the temperature was oscillated sinusoidally by ±2 °C about a mean temperature, the pyroelectric current being monitored continuously over this period. It is easy to show that the pyroelectric coefficient can be computed as follows:

$$p(T) = \frac{i_{0m}}{\Delta T.A.\omega}.\sqrt{\left(\frac{R_e}{R_s}+1\right)^2+\omega^2 R_e^2 C^2} \quad (1)$$

where i_{0m} is the average of the maximum and minimum currents, ω is the angular frequency of temperature oscillation of amplitude ΔT, A is the electrode area, R_e is the resistance of the electrometer (this depends on the instrument range and was taken from the electrometer specification), and R_S is the resistance of the sample, measured as described above and C its capacitance. The advantages of this method in comparison with the Byer–Roundy technique are that it is less susceptible to effects due the thermally stimulated release of trapped charge. Furthermore, it permits consideration of the leakage of charge through the resistance represented by the sample, which can be significant at the high levels of doping. The agreement between the results obtained from the two methods was excellent.

3. Results

Fig. 1 shows a typical SEM image from a ceramic sample, as observed after polishing and etching. The grains are clearly delineated by the etch, which has also revealed the domain structure within the grains. The grain sizes of the Sb and Cr-doped samples as functions of the doping level are shown in Fig. 2. Average errors on the grain size measurement are 10%. It can be seen that both dopants tend act as grain refiners, producing an average grain size of around 4 μm, compared with ca 12 μm in the undoped material. The Curie temperatures measured on heating are shown in Fig. 3. The Cr doped samples show a slight, but non-systematic reduction of

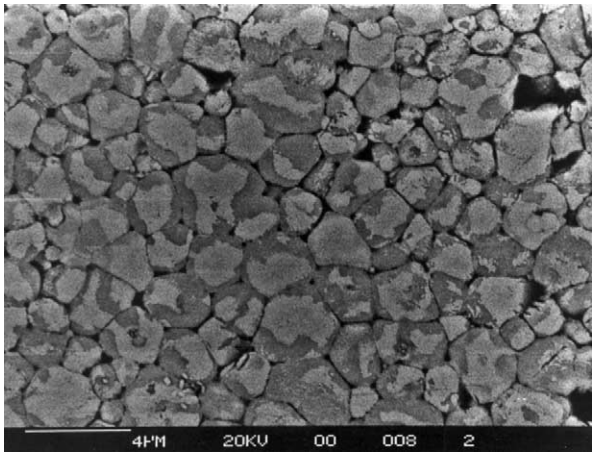

Fig. 1. SEM image of a 1 mol% Cr-doped sample surface after polishing and etching. The scale bar is 4 μm.

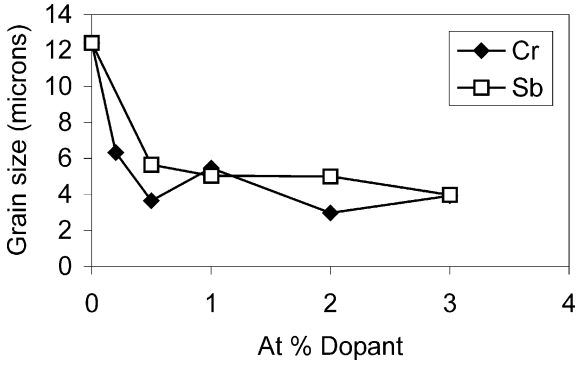

Fig. 2. Grain sizes of Cr and Sb doped ceramics as functions of the doping level.

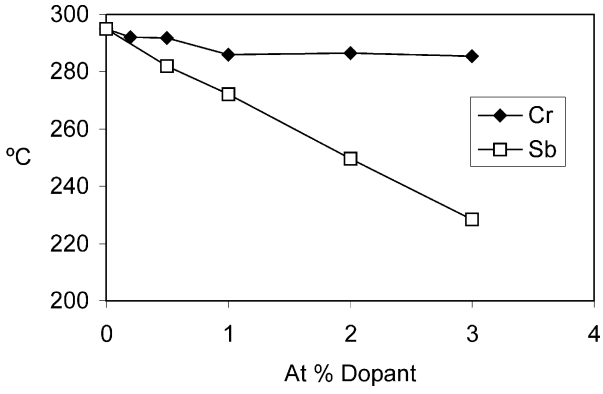

Fig. 3. Curie temperatures (measured on heating) of Cr and Sb doped ceramics as functions of the doping level.

Curie temperature with doping level. The hysteresis in the transition temperature was virtually the same in all samples, averaging at 4 °C. It indicates a weak first-order nature to the transition. The Sb-doped samples, on the other hand, exhibit a linear decrease in Curie temperature with doping level (z) such that $T_C=-22z+294$ °C. In these specimens, the hysteresis was also 4 °C up to 1 at.% Sb, rising to 7 °C for 2 and 3

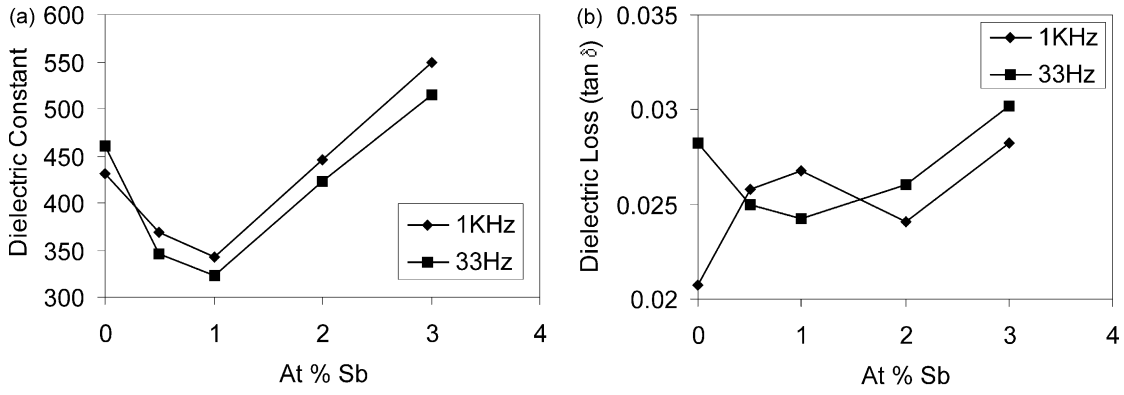

Fig. 4. Dielectric constant (a) and loss (b) of Sb-doped ceramics at 1 kHz and 33 Hz.

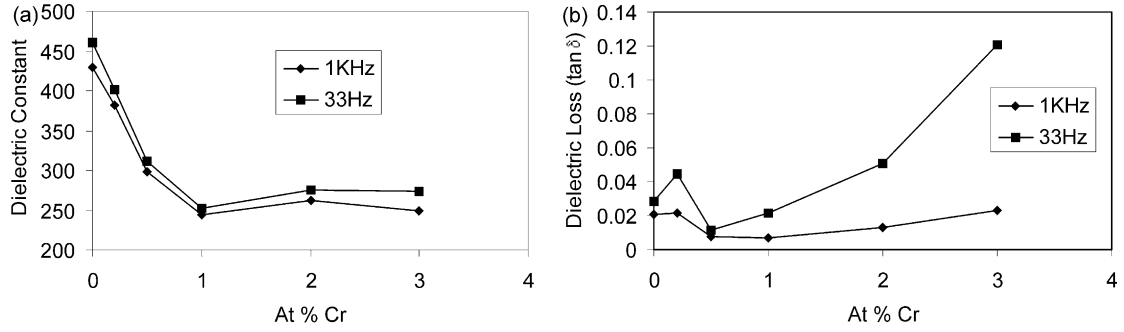

Fig. 5. Dielectric constant (a) and loss (b) of Cr-doped ceramics at 1 kHz and 33 Hz.

at.% Sb. This is also indicative of a first order transition, for which hysteresis would be expected to increase as the transition temperature reduces.

Fig. 4 shows (a) the dielectric constant and (b) the loss tangent at 1 kHz and 33 Hz of poled Sb-doped ceramics as functions of the doping level. Fig. 5 shows the same parameters for poled Cr-doped samples. It can be seen from Fig. 4a that the dielectric constant minimises for both frequencies at around 1 at.% Sb. The loss at 33Hz also minimises at the same level of doping. The loss tangent at 1 kHz shows a slight tendency to rise with increasing frequency. By contrast, there is a dramatic reduction in dielectric constant with increasing doping level for the Cr-doped specimens, at both frequencies. At 1 kHz, there is a tendency for the loss to minimise at between 0.5 and 1 at.% Cr, where it falls to $<1\%$ at 33Hz, the loss also minimises at around 0.5 at.% Cr, and then rises very rapidly above this level of doping. There is a very strong low frequency dependence of the dielectric loss in the range 0.5–3 at.% Cr, probably caused at least to some degree by the contribution of the DC conductivity, which increases markedly in this range of doping level (see below).

Fig. 6 shows the pyroelectric coefficients at 25 °C for the Cr and Sb-doped ceramics. The results reported here are the means of the values obtained from the two measurement methods described above. The average error estimated from distribution of the results from

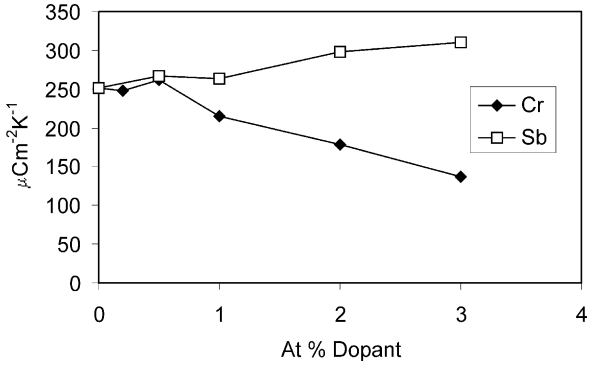

Fig. 6. Pyroelectric coefficients of Cr and Sb-doped ceramics.

these measurements is estimated as being between 2 and 3%. There is an interesting contrast between the Sb and the Cr-doped specimens. The former shows an almost linear increase in the pyroelectric coefficient with increasing Sb content. This is almost certainly related to the monotonic reduction in the Curie temperature over the same range of doping levels reported above and is discussed further below. The Cr-doped specimens, however, show a slight increase in pyroelectric coefficient up to a doping level of 0.5 at.%, followed by a linear reduction.

The dependence of the DC resistivities at 25 °C of the specimens upon doping levels are shown in Fig. 7. The effect of the Sb doping is to increase the resistivity and

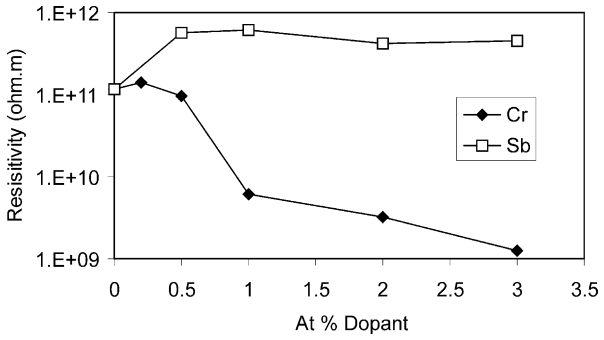

Fig. 7. DC resistivities at 25 °C of Cr and Sb-doped ceramics.

then to hold it at that increased level, with a small reduction in resistivity as the doping level is increased up to 3 at.% Sb. By contrast, the Cr doping first slightly increases the resistivity and then markedly reduces it.

4. Discussion

There are many interesting aspects to the results reported here. The first aspect is the effects of the dopants upon pyroelectric performance. This can be measured in terms of the usual "figures-of-merit" (FOM), defined[2] as $F_V = p/(c'\varepsilon\varepsilon_o)$ and $F_D = p/\{c'(\varepsilon\varepsilon_o \tan\delta)^{1/2}\}$ (where p is the pyroelectric coefficient, c' the volume specific heat, ε the dielectric constant, ε_o the permittivity of free space and $\tan\delta$ the loss tangent). F_V is the relevant FOM for devices in which the device noise is dominated by the readout amplifier. F_D is the relevant FOM when the device noise is dominated by the AC Johnson noise in the element. The computed values of F_V and F_D at 33 Hz are given in Fig. 8 (a) and (b), respectively. First consider the composition dependence of F_V for the Sb doped specimens. A reduction in T_C would be expected to produce an increase in both p and ε. As the temperature of measurement (T) approaches T_C (or vice versa, in this case), then Devonshire theory predicts that $\varepsilon = \alpha/(T_C - T)$ and $p = \beta/(T_C - T)^{1/2}$ and hence $F_V = \gamma(T_C - T)^{1/2}$ (where α, β and γ are constants). By this theory, $p/(\varepsilon)^{1/2}$ should be independent of $(T_C - T)$ so that, at constant $\tan\delta$, the value of F_D should be independent of temperature. At levels of Sb doping of 1 at.% and above, the ratio $p/(\varepsilon)^{1/2}$ varies by less than 3%, indicating that the observed increase in pyroelectric coefficient and dielectric constant in this range are probably determined by the reduction in T_C caused by the doping. Similarly, the increase in the 1 kHz and 33 Hz dielectric losses in this doping range are probably caused by an increased domain wall mobility. Donor ions such as Sb act to reduce the concentration of oxygen vacancies, which will pin the domain walls, and a reduction in T_C will also make the domain walls more mobile. However, the initial reduction in dielectric constant and 33 Hz loss at doping levels up to 1 at.% Sb cannot be explained through the reduction in T_C. A reduction in the number of oxygen vacancies will reduce the number of acceptor centres.[22] It is likely that this initial reduction in permittivity and loss is associated with the consequential reduction in the number of mobile charge carriers in the lattice, a conclusion that is supported by the observed increase in DC resistivity (see Fig. 7). It would also appear from the concentration dependence of the DC resisitivity that the intrinsic level of oxygen vacancies is fully compensated at ca 1 at.% Sb, and above this level the effects of T_C reduction can then be observed in that the permittivity and loss both increase. The changes in F_V and F_D (33 Hz) with composition for the Sb (and Cr) doped specimens are shown in Fig. 8(a) and (b), respectively. It can be seen that there is an increase in F_V of ca 40% in going from the undoped composition to 1 at.% Sb, as the permittivity decreases, followed by a reduction in F_V above 1 at.% Sb as the permittivity increases faster than the pyroelectric coefficient as T_C is reduced. As would be expected from the argument presented above, there is a much smaller change in the value of F_D with composition, the reduction above 1 at.% Sb being associated with the observed increase in loss. The change in resistivity as the Sb level is increased is interesting. As the oxygen vacancies are compensated, the resistivity increases by almost an order-of-magnitude and then stays at this increased level.

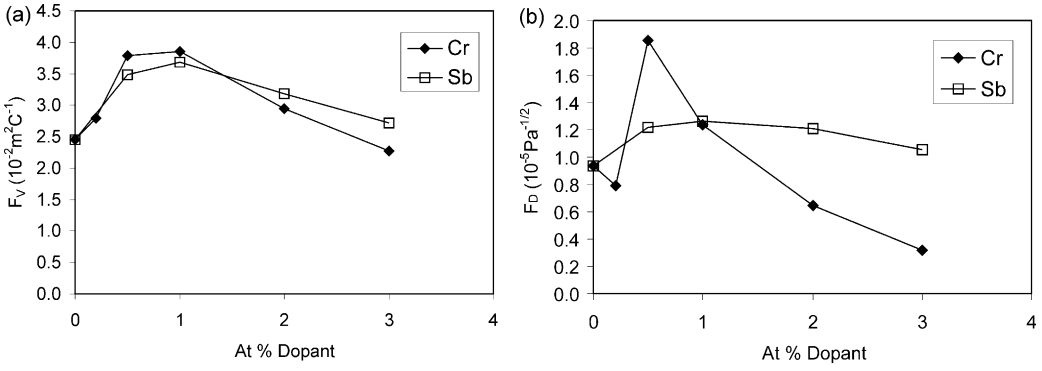

Fig. 8. Pyroelectric figures of merit F_V and F_D for Cr and Sb-doped ceramics. (Assuming that $c' = 2.5\times10^6$ J m^{-3} K^{-1}).

Electronic conduction in the perovskites in this temperature range is entirely determined by carrier hopping between trapping sites.[13,22] Donors or acceptors are not fully ionised, but holes or electrons hop between localised traps. The fact that the resistivity is reasonably independent of the Sb concentration above 1 at.% confirms the hypothesis that the "donor" Sb ions are not ionised, the electrons associated with these dopant sites are trapped, and that therefore we do not see a change to electron-mediated hopping conduction as the Sb ion concentration is increased. Conductivity remains hole-mediated. The conductivity (σ_o) of a ceramic dominated by this form of hopping conduction is given[13] by:

$$\sigma_o = A\exp\left(-\alpha a z^{-1/3} - E_a/kT\right) \quad (2)$$

where A and α are constants, a is the lattice parameter, z is the atomic fraction of trap sites, E_a the activation energy for the hopping process, T the absolute temperature and k is Boltzmann's constant. The "$\exp(-\alpha a z^{-1/3})$" part of this expression is determined by the average hopping distance that a carrier has to traverse between traps and the way it affects the probability of hopping.

Fig. 9 shows a plot of $\ln(\rho)$ vs $1/T$ for the Sb doped specimens. The activation energies determined from the linear portions of these curves (i.e. above 35 °C) are given in Table 1. The E_a does not vary much across the series, confirming that the conduction mechanism does not change across the composition series, and giving an average value of $E_a = 0.59 \pm 0.05$ eV for hole-hopping conduction. This value is not too dissimilar from the value of 0.78 eV for U-doped PZFNTU ceramics at low levels of U-doping, where conductivity is still determined by the intrinsic acceptor level. The fact that the conductivity is only weakly dependent upon the Sb doping level above 1 at.% is presumably because the concentration of acceptor centres does not change much above this doping level, under the synthetic conditions used for the ceramics and so the average distance for hole hopping between the acceptor traps is also unchanged.

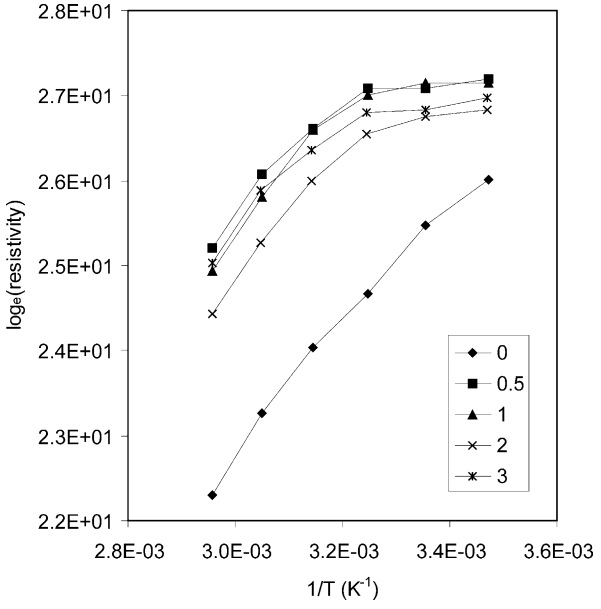

Fig. 9. Log_e(DC resistivity) vs $1/T$ for the Sb-doped ceramics. The legend indicates the doping level for each specimen in at.%.

Table 1
Variation of activation energy for hopping conduction with doping level for Sb-doped ceramics

At.% Sb	Activation energy E_a (eV)
0	0.62
0.5	0.55
1	0.63
2	0.64
3	0.52

By contrast with Sb, Cr would be expected to take a valency of 3+ (it is added as Cr_2O_3) and thus might be expected to sit on the B-site as an acceptor. There is the possibility of Cr existing as Cr^{5+}[23] or even Cr^{6+}, but these would require very strongly oxidising conditions.

If we assume that it is present as Cr^{3+}[24] and is acting as an acceptor, we can understand the effects on the dielectric properties (Fig. 5) as being due firstly to an increase in oxygen vacancies, which will tend to increase the pinning of the domain walls and thus to reduce the dielectric constant and loss up to a doping level of 1 at.%. The loss is then increased (particularly dramatically at 33 Hz) as the DC conductivity is increased. The pyroelectric coefficient (Fig. 6) is also decreased above a level of doping of 1 at.% Cr. This is harder to understand and may not be understood (as for Sb doping) as an intrinsic ferroelectric effect (as the T_C is unchanged). It may be due to the increase in DC conductivity affecting the efficiency of poling, but this needs further work to understand more fully. The consequent effects upon F_V and F_D of the changes in the pyroelectric and dielectric properties are shown in Fig. 8 (a) and (b) respectively. F_V is increased at low doping levels as ε is reduced, but then reduces at higher doping levels as p is reduced. F_D is increased dramatically at low doping levels as ε and $\tan\delta$ are reduced, but is then compromised at the higher doping levels as p reduces and tanδ increases.

The decrease in the DC resistivity (see Fig. 7) with increasing Cr level above 0.2 at.% can be understood in terms of Eq. (2). Fig. 10 shows a plot of $\ln(\sigma_o)$ vs $z^{-1/3}$ (σ_o = DC conductivity) for the Cr-doped ceramics at 25 °C. Here, z is taken as the doping level for the Cr, which assumes that the Cr acceptor sites act as the hole traps. The line is a best fit to the data and gives $\alpha = 0.38$ Å^{-1} (using a lattice parameter determined by powder X-ray diffraction of 4.125 Å). Similar results are obtained at 65 °C. This value of α for hole-hopping

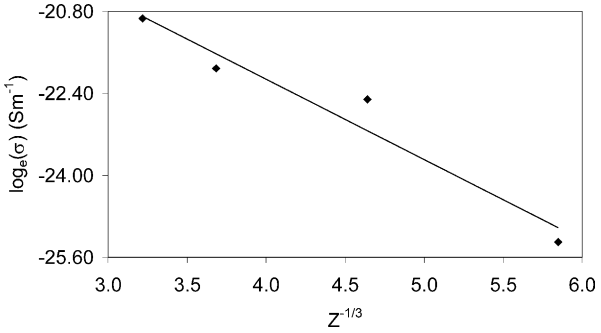

Fig. 10. Variation of loge(DC conductivity) with $z^{-1/3}$ for Cr-doped ceramics.

conduction between Cr-sites compares with values of $\alpha = 0.66$ Å^{-1} determined for electron hopping conduction between U-sites in U-doped PZFNT[13] and $\alpha = 0.63$ Å^{-1} in U-doped PMNZT.[14] The variation of resistivity with temperature for the Cr-doped ceramics is shown in Fig. 11 and the activation energies for conduction in Table 2. It is clear that there is a significant change in activation energy in going from the 0 and 0.2 at.% Cr samples to the 0 samples with 5 at.% Cr and higher. For the first two, the E_a values are very similar to the values obtained with all the Sb doped samples. It can also be seen from the temperature plots that these two samples have very similar resistivities across the range of temperatures explored. These results imply that the sites for the hole traps are the same in both these samples and in the Sb-doped ceramics. Presumably at the 0.2 at.% doping level there are insufficient Cr^{3+} acceptor sites to act as a significant trap for the holes in comparison with the intrinsic hole trapping sites. For the other samples with higher Cr doping levels, the lower activation

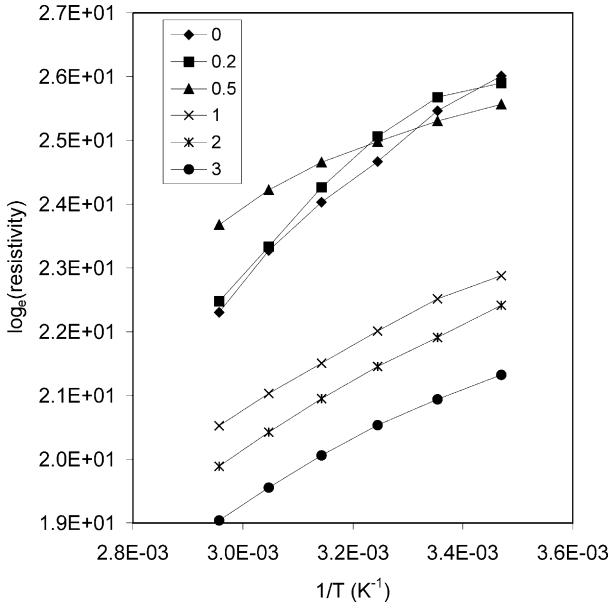

Fig. 11. Log$_e$(DC resistivity) vs $1/T$ for the Cr-doped ceramics. The legend indicates the doping level for each specimen in at.%.

Table 2
Variation of activation energy for hopping conduction with doping level for Cr-doped ceramics

At.% Cr	Activation energy E_a (eV)
0	0.62
0.2	0.59
0.5	0.31
1	0.40
2	0.42
3	0.38

energy for hopping (average 0.38 ± 0.03 eV) coupled with the linear $\ln(\sigma_o)$ vs $z^{-1/3}$ dependence implies that the hole traps are now the Cr^{3+} sites. The E_a measured here is very similar to the values of $E_a = 0.37 \pm 0.01$ eV determined for U-doped PZFNT[13] and 0.28 ± 0.02 eV for U-doped PMNZT[14] ceramics. In these cases, the trapping sites are thought to be for electrons.

5. Conclusions

The electrical properties of Sb and Cr-doped $Pb(Mg_{1/3}Nb_{2/3})_{0.025}(Zr_{0.825}Ti_{0.175})_{0.975}O_3$ ceramics have been studied in detail. Both dopants act as grain refiners. It has been shown that Sb acts as a donor dopant, linearly reducing the Curie temperature and increasing the pyroelectric coefficient and the dielectric constant. At low levels of Sb doping, the dielectric constant and loss are reduced (at both 33 and 100 Hz). The combination of these electrical properties produces 33 Hz pyroelectric FOM's as follows: F_V peaks at 3.8×10^{-2} m^2 C^{-1} and F_D peaks at 1.2×10^{-5} Pa$^{-1/2}$. The dopant concentration dependent behaviour of the FOM and the electrical resistivity have been explained in terms of the changes in T_C and the behaviour of the Sb dopant as a donor ion which reduces oxygen vacancy concentration, but which does not contribute electrons to the conduction process. Cr acts as an acceptor dopant, having little effect on the Curie temperature, but reducing the dielectric constant and loss and markedly reducing the pyroelectric coefficient. Above 0.5 at.% Cr, the resistivity reduces rapidly. The pyroelectric FOM calculations give: F_V peaking at 3.6×10^{-2} m^2 C^{-1} and F_D at 1.9×10^{-5} Pa$^{-1/2}$. The behaviour of Cr as a dopant has been explained in terms of it acting as an acceptor dopant with conduction mediated by the hopping of holes between Cr^{3+} sites.

Acknowledgements

The financial support of EPSRC through grant number GR/L91436/01 is gratefully acknowledged. R.W.W. gratefully acknowledges the financial support of the Royal Academy of Engineering.

References

1. Cooper, J., Minimum detectable power of a pyroelectric thermal receiver. *Rev. Sci. Instrum.*, 1962, **33**, 92–95.
2. Whatmore, R. W., Pyroelectric materials and devices. *Reports on Progress in Physics*, 1986, **49**, 1335–1386.
3. Whatmore, R. W. and Watton, R., Pyroelectric materials and devices. In *Infrared Detectors and Emitters: Materials and Devices*, ed. P. Capper and C. T. Elliott. Chapman and Hall, London, 2000, pp. 99–148.
4. Bennett, M. V. and Matthews, I., Life-saving uncooled IR camera for use in fire-fighting applications. *Proc. SPIE*, 1996, **2744**, 549–554.
5. Hanson, C. M., Beretan, H. R., Belcher, J. F., Udayakumar, K. R. and Soch, K. L., *Proc. SPIE*, 1998, **3379**, 60.
6. Shorrocks, N. M., Whatmore, R. W. and Osbond, P. C., Lead scandium tantalate for thermal detector applications. *Ferroelectrics*, 1990, **106**, 387–392.
7. Kulwicki, B. M., Amin, A., Beratan, H. R. and Hanson, C. M., Pyroelectric imaging. In *Proc. 8th International Symposium on Applications of Ferroelectrics (Greenville, SC, USA 30 August to 2 September 1992 IEEE Cat. No.90CH3080–9)*, 1992, p. 1.
8. Esteve, D., Audaire, L., Bauer, F., Beconne, J. P., Clot, J., Mahrane, A., Pham, V. V. and Simonne, J., Optimisation of a turning passive IR watching detector. *Sensors and Actuators A—Physical*, 1993, **37–8**, 198–201.
9. Binnie, T. D., Weller, H. J., He, Z. Q. and Setiadi, D., An integrated 16×16 PVDF pyroelectric sensor array. *IEEE Trans. UFFC*, 2000, **47**(6), 1413–1420.
10. Fujii, S., Kamada, T., Hayashi, S., Tomita, Y., Takayama, R., Hirao, T., Nakayama, T. and Deguchi, T., *Proc. SPIE*, 2552, **612**.
11. Kohler, R., Padmini, P., Gerlach, G., Hofmann, G. and Bruchhaus, R., *Integrated Ferroelectrics*, 1998, **22**, 383.
12. Bell, A. J. and Whatmore, R. W., Electrical conductivity in uranium-doped modified lead zirconate pyroelectric ceramics. *Ferroelectrics*, 1981, **37**, 543–546.
13. Whatmore, R. W., High performance conducting pyroelectric ceramics. *Ferroelectrics*, 1983, **49**, 201–210.
14. Whatmore, R.W., UK Patent GB2347416A, 2001.
15. Shaw C. P., Gupta S., Stringfellow S. B., Navarro A., Alcock J. R. and Whatmore R. W., Pyroelectric properties of Mn-doped lead zirconate–lead titanate–lead iron niobate ceramics. *J. Eur. Ceram. Soc.*, in press.
16. Stringfellow, S. B., Gupta, S., Shaw, C. P., Alcock, J. R. and Whatmore, R. W., Electrical conductivity control in uranium doped $PbZrO_3$–$PbTiO_3$–$PbMg_{1/3}Nb_{2/3}O_3$ pyroelectric ceramics. *J. Eur. Ceram. Soc.*, 2002, **22**, 573–578.
17. Takahashi, M., Electrical resistivity of lead zirconate titanate ceramics containing impurities. *Jpn. J. Appl. Phys.*, 1971, **10**, 643–651.
18. Lee, Y.-Y., Long, W., Liang, C.-K. and Wu, T.-S., Electrical conductivity in PZT and PT-type piezoceramics. *Ferroelectrics*, 1993, **138**, 11–22.
19. Navarro, A., Shaw, C. P., Alcock, J. R. and Whatmore, R. W., A Taguchi study of defects in the fabrication of PZT ceramics, In: *Proceedings of Ferroelectrics 2000 UK (Congress 2000, Cirencester, April 2000)*, ed. N. McN. Alford and E. Yeatman. IOM Communications Ltd, London, pp. 29–36 (ISBN 1–86125–135–1).
20. Wurst, J. C. and Nelson, J. A., Linear intercept technique for measuring grain size in two-phase polycrystalline ceramics. *J. Am. Ceram. Soc.*, 1972, **55**, 109.
21. Byer, R. L. and Roundy, C. B., *Ferroelectrics*, 1972, **3**, and *IEEE Trans. Sonics Ultrason*, 1972, **SU-19**, 333.
22. Raymond, M. V. and Smyth, D. M., Defects and charge transport in perovskite ferroelecrics. *J. Phys. Chem. Sol.*, 1996, **57**, 1507–1511.
23. Bykov, I. P., Glinchuk, M. D., Skorokhod, V. V., Kurland, V. M., Boudys, M. and Kala, T., The charge state of manganese, titanium and chromium ions and its influence on the properties of the lead titanate-zirconate solid solutions. *Ferroelectrics*, 1992, **127**, 89.
24. Wu, L., Wu, T.-S., Wei, C.-C. and Liu, H.-C., The DC resistivity of modified PZT ceramics. *J. Phys. C: Solid State Phys.*, 1983, **16**, 2823.